Macromolecules

pubs.acs.org/Macromolecules Article

Liquid Crystal Elastomers Prepared by Thiol−Ene Photopolymerization Amenable to Surface-Enforced Alignment

Hayden E. Fowler, Harrison M. Pearl, Jonathan D. Hoang, and Timothy J. White*

Cite This: *Macromolecules* 2024, 57, 2619−2627 Read Online

ACCESS | Metrics & More | Article Recommendations | Supporting Information

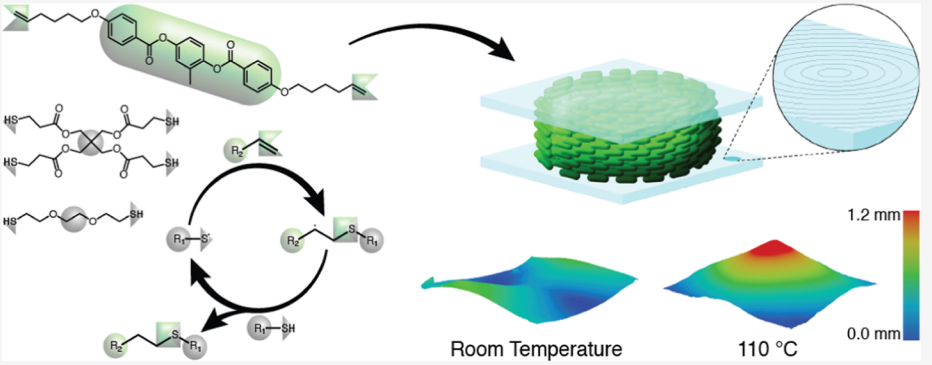

ABSTRACT: Liquid crystal elastomers (LCEs) assimilate the anisotropy of liquid crystalline phases with the rubber elasticity of polymer networks. Numerous recent reports detail the preparation of LCEs by sequential chain extension reactions of diacrylate liquid crystalline monomers followed by the photopolymerization of liquid crystalline oligomers. While these reactions are widely utilized, sample fabrication can take hours or even days. Other reports detail the preparation of LCEs via direct thiol−acrylate photopolymerization via free radical chain transfer reactions. While this is a rapid and straightforward approach to preparing LCEs, the topology of the polymer network composition is heterogeneous, with wide variance in molecular weight between cross-links and extensive prevalence of pendant groups. Here, we detail the preparation of LCEs via thiol−ene photopolymerization. The compositions introduced here are amenable to surface-enforced alignment, which enables the high-fidelity inscription of complex director profiles. Compared to prior thiol-based LCE compositions, direct preparation of LCE by thiol−ene photopolymerization is rapid, forms largely homogeneous polymer networks, and has wide tunability in cross-link density.

INTRODUCTION

Liquid crystal elastomers (LCEs) are soft, stimuli-responsive materials in which liquid crystalline mesogenic units are incorporated into a lightly cross-linked polymer network.[1] Prior research of LCEs has considered the functional utility of their nonlinear deformation[2−4] as well as their stimuli-response (e.g., actuation). Here, we are concerned with the nascent thermotropism of LCEs (e.g., heating LCEs reduces the extent of liquid crystallinity to near zero).[5] De Gennes first predicted the thermotropic character of LCEs as an approach to realized amplified and differentiated thermomechanical response.[6] While LCEs that retain the polydomain orientation exhibit thermomechanical responses, the deformation is uniform in all axes. When LCEs are aligned, the directional deformation of the materials can achieve as much as 50% contractile strain upon heating.[7]

Historically, LCEs have been prepared by two-step hydrosilylation reactions with alignment imparted by mechanical force in the second polymerization stage.[7] More recently, mechanically aligned LCEs are commonly prepared via a two-step process in which diacrylate liquid crystalline monomers (LCMs) are subject to a thiol-Michael addition reaction followed by subsequent photopolymerization of excess acrylate bonds to arrest the LCE in a mechanically deformed state (e.g., aligned).[8] LCEs prepared by thiol-Michael addition have displaced hydrosilylation reactions due to the ease and accessibility of this chemistry. Further, the rheological properties of this material system are conducive to printing via direct ink writing,[9] which has been utilized to produce LCEs with spatial variation in alignment.[10]

While mechanical and rheological methods are widely utilized to prepare aligned LCEs, these methods may be limited in their scalability (mechanical alignment) or patterning fidelity (rheological alignment). Other approaches

Received: November 8, 2023
Revised: February 8, 2024
Accepted: March 4, 2024
Published: March 18, 2024

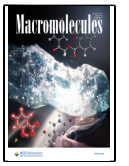

https://doi.org/10.1021/acs.macromol.3c02291
Macromolecules 2024, 57, 2619−2627

have been utilized to enforce alignment to LCEs, including magnetic[11,12] and electric fields as well as surface anchoring. Surface anchoring is widely utilized in the large-scale manufacture of liquid crystal displays and optical films from LCMs.[13] While numerous prior reports detail the preparation of glassy liquid crystalline polymer networks (LCNs) via surface-enforced alignment,[14,15] this technique has only recently been demonstrated for preparing LCEs. In the initial report,[16] LCEs were prepared by photopolymerizing diacrylate liquid crystalline oligomers prepared by an aza-Michael addition reaction. This and subsequent reports utilized photoalignment substrates to prepare LCEs with arbitrarily complex director patterns with a voxel resolution of 10 μm.[17] The fidelity of the photoalignment patterning has been exploited in theory-led experimental demonstrations of complex shape transformations,[18−21] including folding origami.[22]

Other materials chemistries have been subsequently demonstrated to be amenable to surface anchoring, generally utilizing thiol−acrylate reactions.[23,24] In one approach, referred to as free-radical chain transfer, LCEs are prepared from formulations containing diacrylate LCMs and dithiol monomers that act as both chain extenders as well as chain transfer agents.[24−26] This chemistry is robust, strongly anchors to surface coatings, and can be a high throughput as a direct photopolymerization reaction. However, the polymer network formation is heterogeneous, which is evident in distinctive mechanical properties.[25] We have recently demonstrated that adjustment to the kinetics (with comparatively slow base catalysts) of the thiol-Michael addition reaction to prepare oligomeric species can produce aligned LCEs via surface anchoring.[27,28] However, as with LCEs prepared by aza-Michael addition reactions, the oligomerization reaction can occur over hours and limits the throughput of the LCE sample preparation.

The work presented here prepares LCEs in a direct, one-step photopolymerization reaction to produce polymer networks with a regular and robust architecture. This reaction addresses the limitations of other thiol-based approaches to preparing LCEs in that it is rapid, forms homogeneous polymer networks, and is highly tunable. By adjusting the composition of a recently reported materials chemistry to prepare semicrystalline LCEs,[29] we prepare conventional LCEs via direct thiol−ene photopolymerization. This chemistry is amenable to surface-enforced alignment and high throughput (i.e., samples prepared in <1 min). We characterize the reaction and degree of alignment before exploring the tunability of materials properties. The LCE materials examined here exhibit cybotactic nematic phases, which are shown to affect the thermotropic stimuli-response.

EXPERIMENTAL SECTION

Materials. Thiol−ene LCEs were prepared by mixing the photoinitiator 2-benzyl-2-dimethylamino-1-(4-morpholinophenyl)-butanone-1 (I-369, IGM Resins), thiol monomers 2,2′-(ethylenedioxy)diethanethiol (EDDET, Sigma-Aldrich) and pentaerythritol tetrakis(3-mercaptopropionate) (PETMP, Sigma-Aldrich), and liquid crystalline "ene" monomer 2-methyl-1,4-phenylene bis(4-(hex-5-enyloxy)benzoate) (LC2E, SYNTHON Chemicals GmbH&Co., KG). Alignment cells were prepared with either polymeric (Elvamide, DuPont) or photochromic (PAAD 22, Beam Co.) surface treatments.

Alignment Cell Preparation. Alignment cells were prepared by coating glass substrates (Colorado Concepts) with Elvamide. First, the glass substrates were plasma cleaned for 10 min before spin-coating with 0.125 wt % Elvamide in methanol solution at 3500 rpm for 1 min. Coated slides were manually rubbed in one direction with a velvet cloth approximately 30 times. Two glass substrates were glued together by the corners using a Norland optical adhesive mixed with 30 μm silicon bead spacers. The glass slides with rubbed alignment were placed antiparallel (i.e., the rubbed sides faced each other with opposing directions of rubbing). A slight overhang between the substrates was left to allow for the capillary filling process. The assembly was exposed to ultraviolet (UV) light for 3 min to cure the optical adhesive.

LCEs with director profiles described by +1 azimuthal defects were prepared from patterned photoalignment cells. Again, glass substrates were first plasma cleaned for 10 min. Subsequently, substrates were spin-coated with 0.33 wt % PAAD 22 in dimethylformamide solution at 2000 rpm for 1 min. Coated substrates were placed on a hot plate at 100 °C for 30 min to remove residual solvent. The cell assembly was subsequently completed by following the steps outlined above. After assembly, the photoalignment cells were exposed to 445 nm light projected through a diffractive waveplate (Beam Co.).

LCE Fabrication. All LCEs were prepared from compositions utilizing a 1:1 functional group ratio of thiol/ene. The amount of cross-linker incorporated was adjusted by the ratio of PETMP/EDDET in the mixture. The mixture of I-369 and LC2E was melt-mixed at 180 °C. The mixture was set on a hot plate at 100 °C with the alignment cell for 10 min. PETMP and EDDET were added, and the mixture was vortexed for 5 min. The mixture was filled at 100 °C in its isotropic state into the alignment cell via capillary action by depositing the mixture to the overhang of the cell via pipet. After the cell was filled, it was transferred to another hot plate set to 35 °C, in the mixture's nematic state, for 30 min, after which the cell was exposed to 365 nm light at 3 mW cm^{-2} for 5 min to complete polymerization. The cell was soaked in water for 24 h and opened with a razor blade to release the LCE.

Real-Time Infrared Spectroscopy. Real-time infrared spectroscopy (RTIR) was conducted using a custom-built heating stage and a Nicolet iS50 Fourier TIR (FTIR) spectrometer to examine the reaction kinetics of functional group conversion during the reaction. Mixtures were melted and placed between salt plates on a hot plate at 100 °C. The salt plates were moved to the RTIR stage, where the temperature was decreased to 35 °C. The values for the area under the thiol peak (2550−2600 cm^{-1}) and alkene peak (∼1640 cm^{-1}) were recorded approximately every half second. Samples were polymerized for 5 min with 365 nm light. Conversion of functional groups was calculated via eq 1

$$X = \frac{A_i - A_f}{A_i} \tag{1}$$

where X is the conversion, A_i is the area under the peak before polymerization, and A_f is the area under the peak at a given time point after initiating polymerization. These conversions were compared to the theoretical conversion at gelation for a step-growth reaction by eq 2[30]

$$p_c = [r(f_{avg,ene} - 1)(f_{avg,thiol} - 1)]^{-0.5} \tag{2}$$

where p_c is the conversion at gelation, r is the stoichiometric balance of functional groups (in this case, $r = 1$), $f_{avg,ene}$ is the weighted average functionality of alkene-functionalized monomers, and $f_{avg,thiol}$ is the weighted average functionality of thiol-functionalized monomers in the system.

Gel Fractions. Gel fractions of LCEs were taken to confirm the network formation. Samples were weighed initially before soaking in DCM for 72 h. Samples were then dried for 24 h on a hot plate set to 45 °C before weighing again. Gel fractions were calculated according to eq 3

$$f_{gel} = \frac{m_f}{m_i} \tag{3}$$

https://doi.org/10.1021/acs.macromol.3c02291
Macromolecules 2024, 57, 2619−2627

where f_{gel} is the gel fraction, m_f is the final measured mass after soaking in DCM and drying for 24 h, and m_i is the initial measured mass before soaking in DCM.

Polarized Optical Microscopy. LCE alignment was assessed with polarized optical microscopy (POM) using a Nikon Eclipse Ci-Pol instrument with 10× and 20× optical objectives. LCEs were observed at 0, 45, and 90° rotation between crossed polarizers.

X-ray Scattering. The alignment and phase behavior of the LCEs were quantified with wide-angle X-ray scattering (WAXS) and small-angle X-ray scattering (SAXS) via a Xenocs Xeuss 3.0 SAXS/WAXS operating in vacuum and transmission using an 8 keV rotating copper anode. Samples were exposed for 180 s for WAXS scans and 720 s for SAXS scans. Herman's orientation parameter was calculated by eqs 4 and 5

$$S = \frac{1}{2}(3\langle \cos^2 \theta \rangle - 1) \tag{4}$$

$$\langle \cos^2 \theta \rangle = \frac{\int_0^{\pi/2} I(\theta) \sin \theta \cos^2 \theta \, d\theta}{\int_0^{\pi/2} I(\theta) \sin \theta \, d\theta} \tag{5}$$

where S is Herman's orientation parameter, θ is the azimuthal angle, and $I(\theta)$ is the azimuthal intensity distribution. Equation 5 gives the average angle of liquid crystalline mesogens relative to the nematic director. Cybotactic nematic phase parameters, including smectic C layer spacing, tilt angle, and cell length, were calculated from SAXS patterns using eqs 6, 7, and 8

$$d = \frac{2\pi}{q_{SAXS}} \tag{6}$$

$$\beta = \frac{\theta_2 - \theta_1}{2} \tag{7}$$

$$L = \frac{d}{\cos \beta} \tag{8}$$

where d is the smectic C layer spacing, q_{SAXS} is the q value at which the maximum intensity occurs in the small-angle region of interest, β is the tilt angle of smectic C layers to the nematic director, θ_1 and θ_2 are the angles of maximum intensity for the pair of diffuse arcs in the cybotactic SAXS pattern, and L is the cell length of smectic layers.

Differential Scanning Calorimetry. Differential scanning calorimetry (DSC) was conducted using TA Instruments' DSC 2500 to determine the thermal properties of LCEs. A heat−cool-heat cycle was applied to the samples at a heating and cooling rate of 5 °C min^{-1}. Glass transition temperatures were obtained by the midpoint of the step change in the baseline on the second heating curve. The temperature at which the local maximum of the peak occurs on the second heating curve identified nematic-to-isotropic transition temperatures.

Tensile Testing. Mechanical properties were measured with a TA Instruments' DMA 850 dynamic mechanical analyzer. Tensile testing was performed on monodomain samples with strips cut perpendicular to and parallel to the nematic director. Samples were tested in rectangular strips with dimensions of approximately 2 mm width and 6 mm length. Tensile tests were performed to failure at room temperature with a linear strain rate of 5% min^{-1} of the original sample length. Young's modulus values were taken from the linear region of the tensile curve at low strain values (1−3%). Modulus contrast was calculated as the ratio between Young's modulus parallel and perpendicular to the alignment direction.

Thermomechanical Response. Thermomechanical testing was performed on monodomain samples using a DMA 850 and tension clamps. The sample was oriented such that the alignment was normal to that of the clamps. The stress on the sample was maintained at approximately 0 MPa, and the contractile strain was tracked as the sample was ramped from room temperature to 220 °C at a rate of 5 °C min^{-1}.

POM, WAXS, and SAXS were also performed for samples heated discretely from room temperature to 220 °C. Samples were heated with an INSTEC thermal stage for POM experiments. SAXS and WAXS profiles were obtained using a Xenocs Xeuss 3.0 SAXS/WAXS equipped with a Linkam thermal stage.

The deformation of LCEs with +1 azimuthal defect alignment in 3 dimensions was characterized via a Keyence VR-3200 wide-area 3D measurement system. Height maps were produced to characterize the LCEs' shape profile and quantify the amount of deformation.

RESULTS AND DISCUSSION

LCEs were prepared by one-step thiol−ene photopolymerization of the liquid crystal monomer LC2E and thiol monomers PETMP and EDDET (Figure 1A). The thiol−ene reaction is

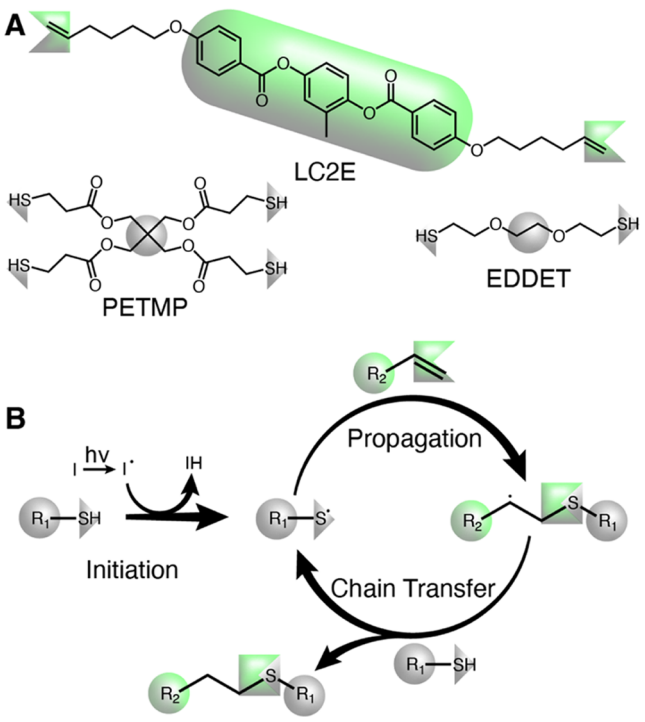

Figure 1. (A) Alkene-functionalized liquid crystalline monomer LC2E was copolymerized with thiol-functionalized monomers PETMP and EDDET via (B) thiol−ene photopolymerization.

outlined in Figure 1B and has been widely reviewed elsewhere.[31,32] The copolymerization of difunctional alkene and thiol monomers results in linear polymer chains. Increasing the average functionality of the composition to greater than two by including multifunctional thiol or ene (typically trifunctional or tetrafunctional) monomers results in a cross-linked network. Here, LC2E and EDDET (both difunctional) react to form linear linkages (i.e., increase the molecular weight between cross-links) that react with the cross-linker PETMP (tetrafunctional). The chemistry presented here builds upon a recent report preparing semicrystalline LCEs by thiol−ene photopolymerization.[29]

Thiol−ene polymerizations can produce cross-linked polymer networks with widely tunable properties. Here, by adjusting the relative amounts of EDDET to PETMP (while maintaining a constant 1:1 thiol/ene stoichiometric ratio of functional groups), we can readily adjust the extent of cross-linking in LCEs prepared with constant liquid crystalline content. This is notable, as (1) maximizing liquid crystalline content is critical to enabling amenability to surface alignment

https://doi.org/10.1021/acs.macromol.3c02291
Macromolecules 2024, 57, 2619−2627

and (2) the liquid crystalline concentration is directly correlated to the magnitude and rate of thermomechanical response.[33−35] The compositions examined in this work are summarized in Table S1 (Supporting Information). As the concentration of EDDET and PETMP was commensurately adjusted, the cross-linker content increased from approximately 14 to 29 mol %. The relative mass fraction (reported here as wt %, Table S1) of liquid crystal monomer changes very little between formulations (from 67 to 70 wt %). As a result, the phase behavior of these compositions is similar and allows materials to be prepared under identical conditions (35 °C) in the nematic phase.

The conversion of thiol and alkene functional groups was monitored with RTIR spectroscopy during photopolymerization (Figure 2). The alkene (Figure 2A) and thiol (Figure 2B)

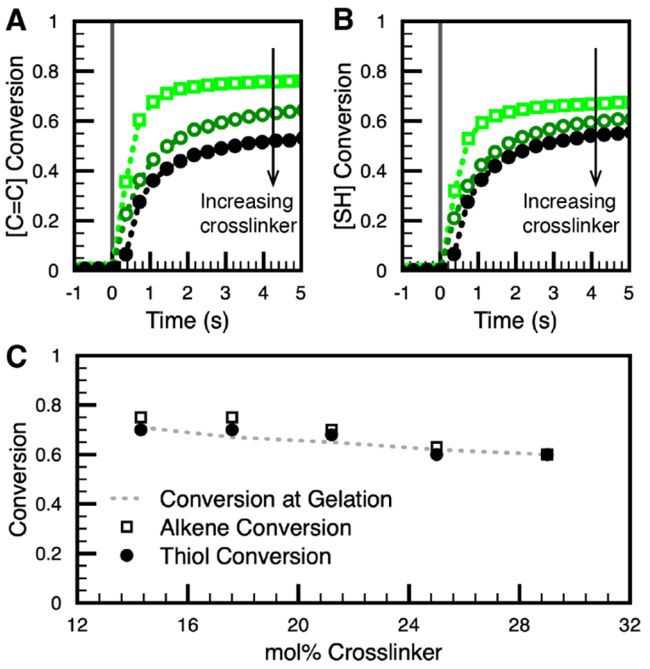

Figure 2. (A) Alkene and (B) thiol functional group conversion during the initial 5 s of photopolymerization for LCE compositions prepared with 14 (hollow light green squares), 21 (hollow dark green circles), and 29 (filled black circles) mol % PETMP. (C) Overall functional group conversion maps to the calculated gel point conversion.

functional group conversions are presented during the first 5 s of photopolymerization for three concentrations of PETMP. Increasing the concentration of cross-linker reduces both thiol and ene conversion. Comparing the slope of conversion−time data in the linear region indicates that the reaction rate decreases with more cross-linker addition. Comparatively, LCEs prepared with lower cross-linker concentration have slightly more conversion of alkene functional groups than thiol functional groups. This potentially indicates a minor extent of homopolymerization of LC2E. However, the polymer network is formed by thiol−ene bonds via step-growth polymerization. While the overall conversion is low, the measured gel fractions are high (>90% in all cases, Table S2).

Notably, in this study, the composition includes an aliphatic diene, an aliphatic dithiol, and a mercaptopropionate tetrathiol. Canonical studies of thiol−ene polymerizations emphasize that the reaction of mercaptopropionate thiols can proceed at nearly 6 times the rate of aliphatic thiols.[32] Unfortunately, we cannot distinguish the reaction kinetics of these distinct thiol groups in this composition, but we can assess the overall thiol−ene polymerization with RTIR.

The conversion of both thiol and ene functional groups can be affected by cross-linker concentration and the associated influence on gel point conversion. We use eq 2 to predict the conversion at gelation. As evident in Figure 2C, the experimentally measured conversions closely match the calculated gel point conversions. From these data, we can conclude that the thiol−ene reaction is generally conventional and proceeds rapidly on initiation, requiring less than 1 min of photopolymerization to reach near the maximal conversion of functional groups (see Figure S1, Supporting Information).

Thiol−ene photopolymerization offers a straightforward and rapid approach to preparing LCEs that are amenable to surface alignment. A recent report of a similar composition detailed the preparation of semicrystalline LCEs.[29] Here, we adjust the composition to prepare LCEs with a monodomain alignment. This study enforces alignment by drawing the liquid crystalline monomer melt into an alignment cell. The material aligns with the rubbing direction of the alignment layers in the nematic phase. Photoinitiation of the monomeric mixture in the aligned nematic phase forms an LCE that retains monodomain alignment. We assess the degree of alignment via polarized optical microscopy (POM) in Figure 3A, where the birefringence of monodomain LCEs is illustrated for a representative sample with 14 mol % PETMP (see Figure S2 for other samples). Alignment was also quantified with X-ray scattering at wide angles (WAXS) for LCEs prepared with 14, 21, and 29 mol % PETMP. Figure 3B shows a representative scattering pattern of LCEs prepared with 14 mol % PETMP (see Figure S3 for other samples). The characteristic nematic eyebrow evident in Figure 3B confirms the alignment. The orientation parameter was calculated from the azimuthal intensity profile (via eqs 4 and 5) and ranged from 0.51 to 0.56 (see Table S3). These values confirm strong nematic alignment similar to values reported in other LCEs prepared by surface alignment.[16,24,27,28]

The microstructure is evident in the polarized micrographs with regular striation normal to the direction of alignment (Figures 3C and S4). Further, the wide-angle X-ray scattering (WAXS) pattern in Figure 3B contains multiple faint, diffuse arcs at smaller angles, indicating additional liquid crystalline ordering.[36] To elucidate the phase retention of these LCEs, we collected small-angle X-ray scattering (SAXS) patterns. Figure 3D shows the SAXS pattern of a representative sample with 14 mol % PETMP (see Figure S5 for other samples). Four diffuse rod-shaped scattering arcs are present, with the top and bottom pairs overlapping a faint nematic scattering arc at constant q oriented along the alignment direction and coincident with the length of the liquid crystalline mesogen. This scattering pattern is associated with the cybotactic nematic phase (illustrated in Figure 3E), in which a nematic phase has regions of short-range smectic order.[37] In these domains, the liquid crystalline mesogens maintain orientational ordering along the director, but tilted smectic C-like phases form. We refer to the angle between the director and the layer normal as the tilt angle and the thickness of the layers as the cell length, which is usually on the order of magnitude of the extended liquid crystalline component.[38] The cybotactic nematic phase has been retained in liquid crystal polymer materials, including LCEs.[24,25,38−44] Average smectic C

https://doi.org/10.1021/acs.macromol.3c02291
Macromolecules 2024, 57, 2619−2627

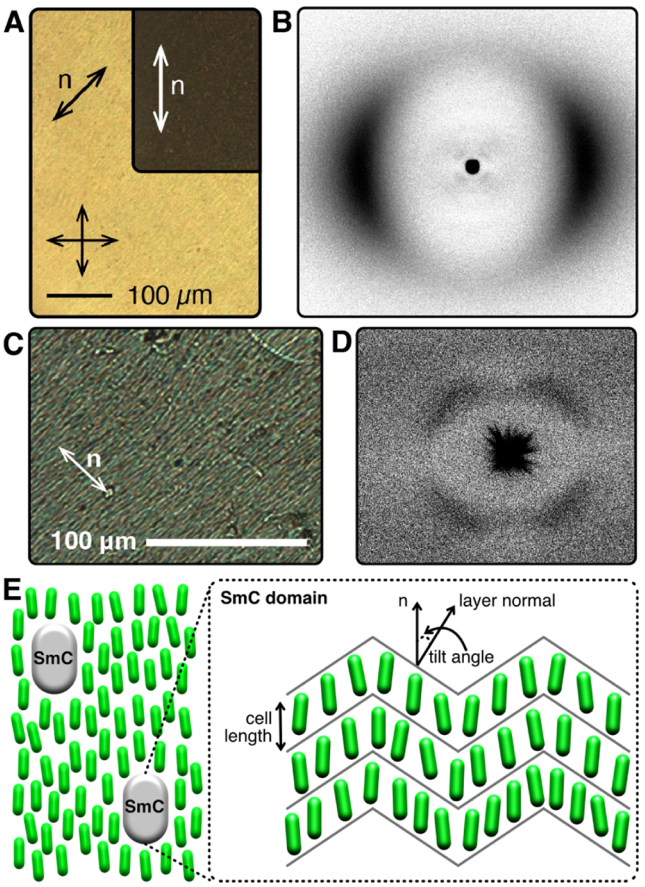

Figure 3. (A) Polarized micrograph of an LCE prepared with 14 mol % PETMP with a 10× objective. (B) X-ray scattering pattern at wide angles illustrating the classic nematic eyebrow pattern indicative of uniaxial alignment. (C) Polarized micrograph with a 20× objective illustrating the microstructure normal to the alignment direction. (D) X-ray scattering pattern at small angles confirming the (E) cybotactic nematic phase consisting of smectic C domains within an overall nematic matrix.

domain layer spacing, tilt angle, and cell length are given for samples with three different concentrations of PETMP in Table S3. The cell lengths are on the order of the extended liquid crystalline unit length (ca. 36.7 Å).

Increasing the cross-linker concentration in the LCEs adjusts the thermomechanical properties. DSC measurements of the LCEs confirm that, as expected, increasing the cross-linker concentration increases the glass transition temperature (Figure 4A,B). The glass transition temperatures for the LCEs examined here are below room temperature. At higher temperatures, the LCEs exhibit a nematic−isotropic transition. Increasing the cross-linker concentration increases the nematic−isotropic transition temperature of the LCE (Figure 4C). Furthermore, the increase in cross-link density also broadens the transition due to a decrease in mobility and potential differences in orientational order (Figure S3 and Table S3).

The mechanical properties of the LCEs were examined with tensile testing parallel and perpendicular to the nematic director. When the LCEs are deformed parallel to the alignment direction, the stress−strain response is classical (Figure 5A). Notably, increasing cross-linker concentration sharpens strain hardening. As expected, the stress−strain response of the LCEs is nonlinear when deformed perpendicular to the alignment direction, previously referred to as soft elasticity.[2,45] Increasing cross-linker concentration sharpens strain hardening and shifts this region to lower strain values. The stress threshold to induce soft elasticity and the extent of the soft elastic plateau also increase with increasing cross-linker concentration. To illustrate the influence of cross-linker concentration on the mechanical properties of the LCEs, we measured Young's moduli in the linear regime in both directions (summarized in Figure 5C). Unsurprisingly, increasing cross-link density increases the Young's moduli in both axes. To assess the influence of cross-linker concentration on the mechanical properties of the LCE, we also calculate what we refer to as the modulus contrast ($Y_{\parallel}/Y_{\perp}$). As evident in Figure 5D, increasing the cross-linker concentration increases the modulus contrast.

The thermotropic stimuli response of LCEs parallel to the alignment direction was examined. Monodomain LCEs were heated from room temperature beyond the nematic−isotropic transition peak observed via DSC (Figure 4). The contractile strain was measured in tension along the aligned direction (Figure 6A) for LCEs prepared with 14, 21, and 29 mol % PETMP. As more cross-linkers are incorporated into the system, the contractile strain response shifts to higher temperatures. Notably, increasing cross-linker concentration does not affect the magnitude of the achievable strain. Close examination of the thermomechanical curve shape of the LCEs prepared with 14 and 21 mol % PETMP reveals that the response has two separate slopes. This is best visualized by taking the derivative of the strain-temperature curves (Figure 6B). As cross-linker content is decreased, the lower temperature response becomes broader and starts at lower temper-

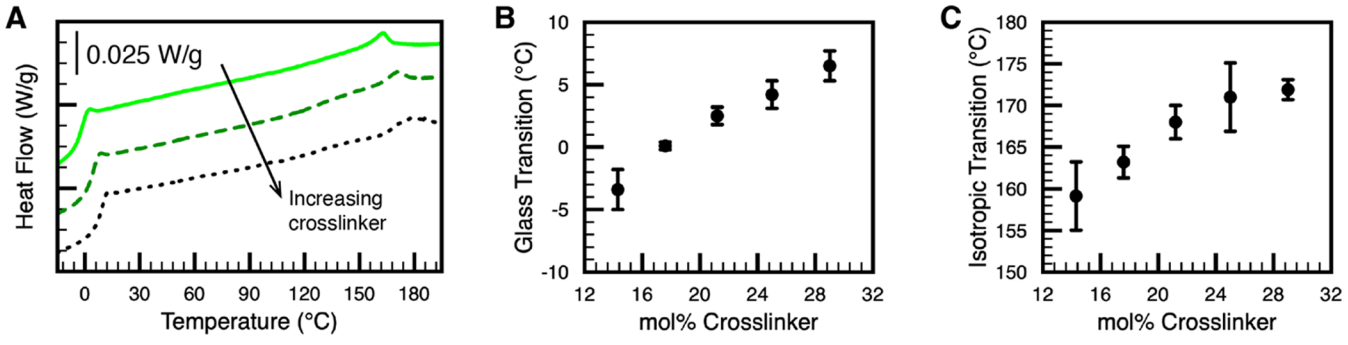

Figure 4. (A) DSC thermograms of LCEs prepared with 14 (solid, light green), 21 (dashed, dark green), and 29 (dotted black) mol % PETMP. The (B) glass transition temperature and (C) nematic−isotropic transition temperature increase with cross-linker concentration.

https://doi.org/10.1021/acs.macromol.3c02291
Macromolecules 2024, 57, 2619−2627

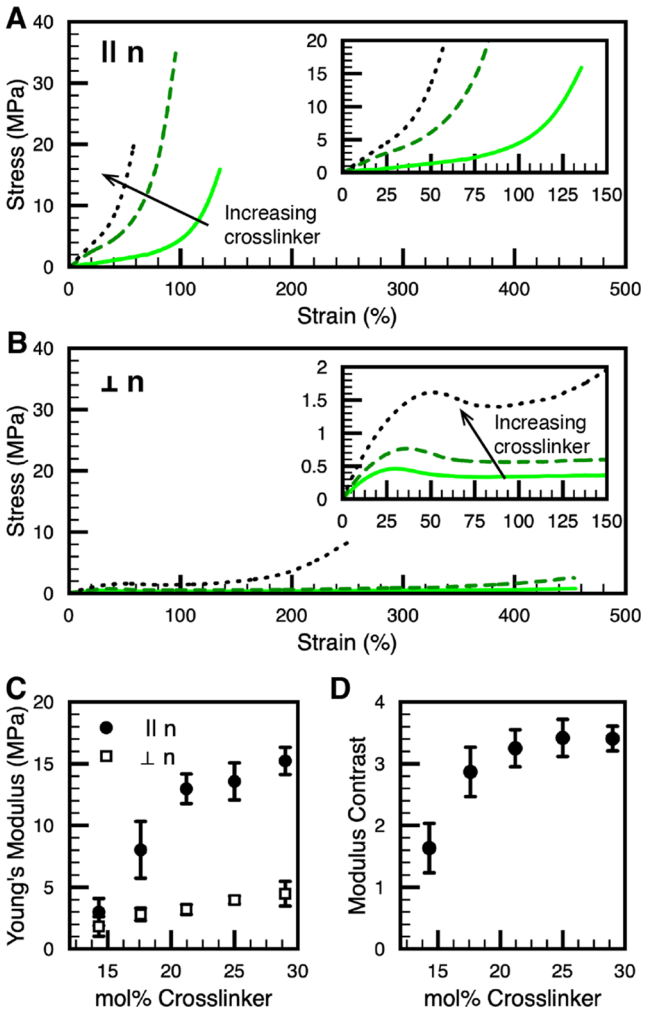

Figure 5. Tensile curves (A) parallel and (B) perpendicular to the direction of alignment for uniaxially aligned LCEs prepared with 14 (solid, light green), 21 (dashed, dark green), and 29 (dotted black) mol % PETMP. (C) Young's modulus for deformation parallel and perpendicular to the nematic director as a function of cross-linker concentration. (D) Modulus contrast ($Y_{\parallel}/Y_{\perp}$) of LCEs as a function of cross-linker concentration.

atures. Interestingly, this initial transition does not appear in the DSC thermograms. The second response region aligns with the nematic−isotropic transition temperature determined by DSC.

POM, SAXS, and WAXS experiments were performed on LCEs prepared with 14 mol % PETMP heated through the nematic−isotropic transition temperature. The POM micrographs in Figure 7A show that the LCE maintains birefringence through the first transition (up to 160 °C) before losing almost all of the birefringence during the second transition (up to 220 °C). This is consistent with the nematic−isotropic transition observed via DSC as shown in Figure 4. The WAXS profiles in Figure 7B confirm that the LCE remains aligned through the first transition before losing alignment during the second transition. The SAXS profiles in Figure 7C indicate that the initial stimuli-response may be associated with the cyclotactic nematic phase. As with the evolution of the nematic phase, the small-angle peaks associated with the cybotactic nematic phase become fainter in the second transition. Data presented in Figure 7D,E give the corresponding intensity profiles as a

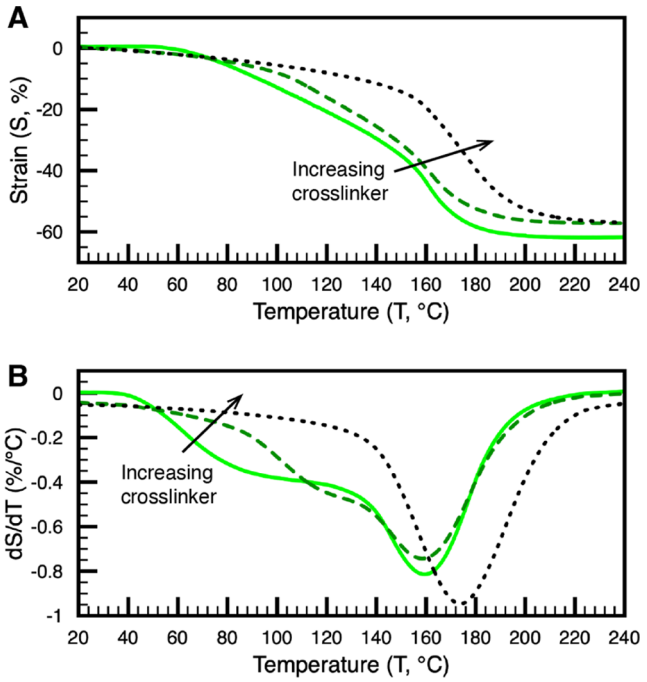

Figure 6. (A) Thermomechanical contractile strain response as a function of temperature and (B) corresponding derivative for LCEs prepared with 14 (solid, light green), 21 (dashed, dark green), and 29 (dotted black) mol % PETMP.

function of azimuthal angle (designated by the red dashed lines in the first image of Figure 7B,C) in the wide-angle and small-angle regions, respectively. From 35 to 100 °C, both intensity profiles become sharper, indicating improved alignment of the cybotactic nematic phase. On increasing the temperature is increased to 160 °C, the sharpness decreases. A considerable decrease is apparent at 220 °C during the second transition, although as with the POM image in Figure 7A, there is evidence that a small amount of alignment remains likely associated with the paranematic state of this material.

Finally, to illustrate the amenability of these material compositions to complex director patterns, we subject these materials to alignment cells prepared with director profiles in *a* + 1 azimuthal defect (via photoalignment). Upon heating, the LCEs go from flat to 3D, forming a cone (Figure 8A). The images presented in Figure 8A are 3D height maps of the deformation of the LCE at room temperature and 110 °C. The LCE at room temperature has a slight saddle-like shape.[46] On heating, the LCE deforms into a cone, where the height increases with increasing temperature (Figure 8B). The deformation produces a classic cone-like shape with positive Gaussian curvature (Figure 8C) when viewing the profile from one side (down the *Y*-axis at the *Z*−*X* plane, as labeled in Figure 8A).

CONCLUSIONS

This report details the preparation of LCEs via thiol−ene photopolymerization. The compositions reported here are subject to surface-enforced alignment. The materials chemistry has advantages in processability and throughput. Furthermore, cross-linking is readily adjusted in the materials by adjusting the ratio of thiol monomers. This report systematically and exhaustively characterizes the material properties and phase behavior. Notably, the LCEs retained the cybotactic nematic

https://doi.org/10.1021/acs.macromol.3c02291
Macromolecules 2024, 57, 2619−2627

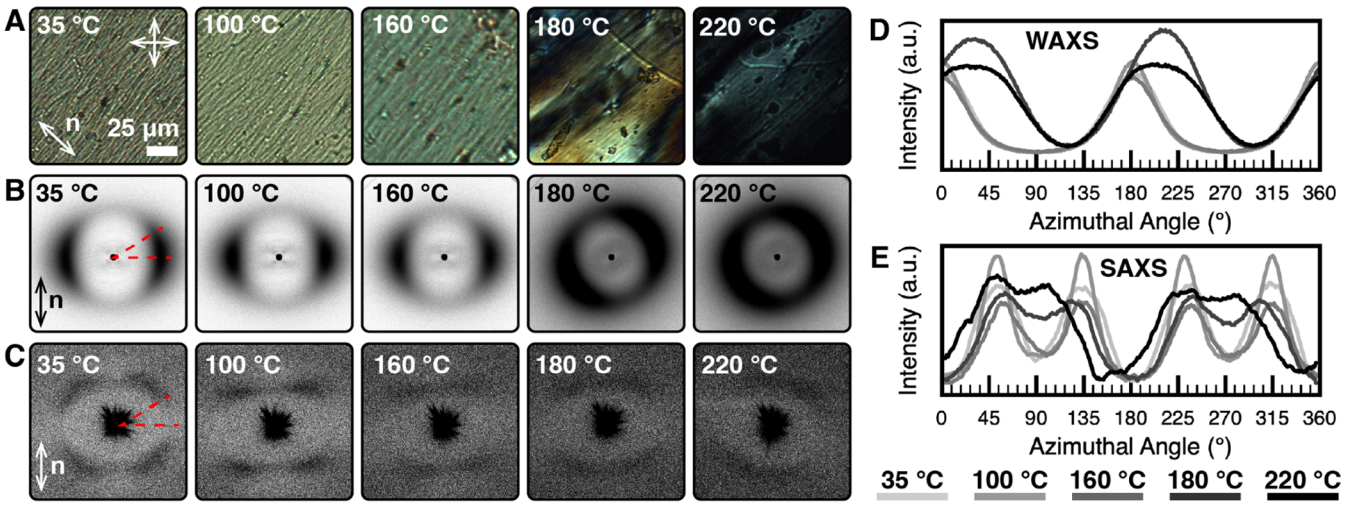

Figure 7. (A) POM, (B) WAXS, and (C) SAXS as a function of temperature for LCEs prepared with 14 mol % PETMP. (D) WAXS and (E) SAXS intensity profiles as a function of azimuthal angle (illustrated by the red dashed lines in the first images of (B, C)).

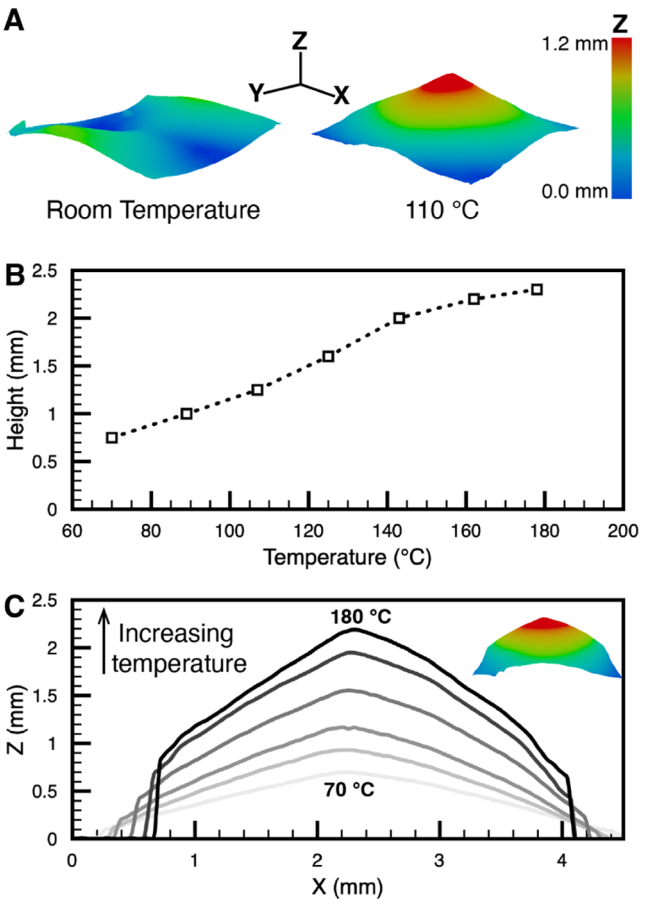

Figure 8. (A) Room-temperature saddle conformation transitions to a cone deformation at 110 °C, illustrated by the 3D height map. (B) Cone height increases as a function of temperature. (C) Cone-like deformation results in positive Gaussian curvature.

phase. The stimuli-response of these LCEs has two distinct regions consisting of a slow and extended low-temperature response, followed by a rapid higher-temperature response. This study details another facile and accessible materials chemistry used to prepare LCEs to enable functional utility in robotics, medicine, and energy.

■ ASSOCIATED CONTENT

Supporting Information

The Supporting Information is available free of charge at https://pubs.acs.org/doi/10.1021/acs.macromol.3c02291.

Formulation compositions; real-time conversion; gel fractions; additional POM, WAXS, and SAXS; average orientation and cybotactic nematic parameters (PDF)

■ AUTHOR INFORMATION

Corresponding Author

Timothy J. White − *Department of Chemical and Biological Engineering, University of Colorado Boulder, Boulder, Colorado 80309, United States; Materials Science and Engineering Program, University of Colorado Boulder, Boulder, Colorado 80309, United States;* orcid.org/0000-0001-8006-7173; Email: timothy.j.white@colorado.edu

Authors

Hayden E. Fowler − *Department of Chemical and Biological Engineering, University of Colorado Boulder, Boulder, Colorado 80309, United States*

Harrison M. Pearl − *Department of Chemical and Biological Engineering, University of Colorado Boulder, Boulder, Colorado 80309, United States*

Jonathan D. Hoang − *Materials Science and Engineering Program, University of Colorado Boulder, Boulder, Colorado 80309, United States*

Complete contact information is available at: https://pubs.acs.org/10.1021/acs.macromol.3c02291

Author Contributions

The manuscript was written through the contributions of all authors. All authors have approved the final version of the manuscript.

Notes

The authors declare no competing financial interest.

■ ACKNOWLEDGMENTS

The authors thank Prof. Taylor Ware, Dr. Mahjabeen Javed, and Dr. Joselle McCracken for their insight and helpful conversations. H.E.F. acknowledges fellowship support from

the National Science Foundation's Graduate Research Fellowship Program (NSF GRFP). The authors also acknowledge financial support from Sandia National Laboratories and National Science Foundation DMR grant 2105369. This work utilized a Xenocs Xeuss 3.0 X-ray system purchased by Department of Defense grant N00014-22-1-2361.

■ ABBREVIATIONS

LCE, liquid crystal elastomer; RTIR, real-time IR; POM, polarized optical microscopy; WAXS, wide-angle X-ray scattering; SAXS, small-angle X-ray scattering; DSC, differential scanning calorimetry; PETMP, pentaerythritol tetrakis(3-mercaptopropionate); EDDET, 2,2′-(ethylenedioxy)diethanethiol; LC2E, 2-methyl-1,4-phenylene bis(4-(hex-5-enyloxy)benzoate)

■ REFERENCES

(1) Herbert, K. M.; Fowler, H. E.; McCracken, J. M.; Schlafmann, K. R.; Koch, J. A.; White, T. J. Synthesis and Alignment of Liquid Crystalline Elastomers. *Nat. Rev. Mater.* **2022**, *7*, 23−38.
(2) Dey, S.; Agra-Kooijman, D. M.; Ren, W.; McMullan, P. J.; Griffin, A. C.; Kumar, S. Soft Elasticity in Main Chain Liquid Crystal Elastomers. *Crystals* **2013**, *3* (2), 363−390.
(3) Kundler, I.; Finkelmann, H. Strain-induced Director Reorientation in Nematic Liquid Single Crystal Elastomers. *Macromol. Rapid Commun.* **1995**, *16* (9), 679−686.
(4) Finkelmann, H.; Greve, A.; Warner, M. The Elastic Anisotropy of Nematic Elastomers. *Eur. Phys. J. E* **2001**, *5* (3), 281−293.
(5) Warner, M.; Terentjev, E. M. Nematic Elastomers - A New State of Matter? *Prog. Polym. Sci.* **1996**, *21* (5), 853−891.
(6) De Gennes, P. G. Possibilites Offertes Par La Reticulation de Polymeres En Presence d'un Cristal Liquide. *Phys. Lett. A* **1969**, *28* (11), 725−726.
(7) Küpfer, J.; Finkelmann, H. Nematic Liquid Single Crystal Elastomers. *Makromol. Chem., Rapid Commun.* **1991**, *12*, 717−726.
(8) Yakacki, C. M.; Saed, M.; Nair, D. P.; Gong, T.; Reed, S. M.; Bowman, C. N. Tailorable and Programmable Liquid-Crystalline Elastomers Using a Two-Stage Thiol-Acrylate Reaction. *RSC Adv.* **2015**, *5* (25), 18997−19001.
(9) Bauman, G. E.; Koch, J. A.; White, T. J. Rheology of Liquid Crystalline Oligomers for 3-D Printing of Liquid Crystalline Elastomers. *Soft Matter* **2022**, *18* (16), 3168−3176.
(10) Ambulo, C. P.; Burroughs, J. J.; Boothby, J. M.; Kim, H.; Shankar, M. R.; Ware, T. H. Four-Dimensional Printing of Liquid Crystal Elastomers. *ACS Appl. Mater. Interfaces* **2017**, *9* (42), 37332−37339.
(11) Yang, H.; Buguin, A.; Taulemesse, J. M.; Kaneko, K.; Méry, S.; Bergeret, A.; Keller, P. Micron-Sized Main-Chain Liquid Crystalline Elastomer Actuators with Ultralarge Amplitude Contractions. *J. Am. Chem. Soc.* **2009**, *131* (41), 15000−15004.
(12) Li, M. H.; Keller, P.; Yang, J.; Albouy, P. A. An Artificial Muscle with Lamellar Structure Based on a Nematic Triblock Copolymer. *Adv. Mater.* **2004**, *16* (21), 1922−1925.
(13) Broughton, B. Surface Alignment of Liquid Crystals. In *Handbook of Liquid Crystals*; Wiley-VCH Verlag GmbH & Co. KGaA, 2014; pp 1−22.
(14) McConney, M. E.; Tondiglia, V. P.; Hurtubise, J. M.; Natarajan, L. V.; White, T. J.; Bunning, T. J. Thermally Induced, Multicolored Hyper-Reflective Cholesteric Liquid Crystals. *Adv. Mater.* **2011**, *23* (12), 1453−1457.
(15) Harris, K. D.; Cuypers, R.; Scheibe, P.; Van Oosten, C. L.; Bastiaansen, C. W. M.; Lub, J.; Broer, D. J. Large Amplitude Light-Induced Motion in High Elastic Modulus Polymer Actuators. *J. Mater. Chem.* **2005**, *15* (47), 5043−5048.
(16) Ware, T. H.; McConney, M. E.; Wie, J. J.; Tondiglia, V. P.; White, T. J. Voxelated Liquid Crystal Elastomers. *Science* **2015**, *347* (6225), 982−984.
(17) Kowalski, B. A.; Tondiglia, V. P.; Guin, T.; White, T. J. Voxel Resolution in the Directed Self-Assembly of Liquid Crystal Polymer Networks and Elastomers. *Soft Matter* **2017**, *13* (24), 4335−4340.
(18) Plucinsky, P.; Kowalski, B. A.; White, T. J.; Bhattacharya, K. Patterning Nonisometric Origami in Nematic Elastomer Sheets. *Soft Matter* **2018**, *14* (16), 3127−3134.
(19) Kowalski, B. A.; Mostajeran, C.; Godman, N. P.; Warner, M.; White, T. J. Curvature by Design and on Demand in Liquid Crystal Elastomers. *Phys. Rev. E* **2018**, *97* (1), No. 012504.
(20) Plucinsky, P.; Lemm, M.; Bhattacharya, K. Programming Complex Shapes in Thin Nematic Elastomer and Glass Sheets. *Phys. Rev. E* **2016**, *94* (1), No. 010701.
(21) Mostajeran, C.; Warner, M.; Ware, T. H.; White, T. J. Encoding Gaussian Curvature in Glassy and Elastomeric Liquid Crystal Solids. *Proc. R. Soc. A* **2016**, *472* (2189), No. 20160112.
(22) Fuchi, K.; Ware, T. H.; Buskohl, P. R.; Reich, G. W.; Vaia, R. A.; White, T. J.; Joo, J. J. Topology Optimization for the Design of Folding Liquid Crystal Elastomer Actuators. *Soft Matter* **2015**, *11* (37), 7288−7295.
(23) Ware, T. H.; Perry, Z. P.; Middleton, C. M.; Iacono, S. T.; White, T. J. Programmable Liquid Crystal Elastomers Prepared by Thiol-Ene Photopolymerization. *ACS Macro Lett.* **2015**, *4* (9), 942−946.
(24) Godman, N. P.; Kowalski, B. A.; Auguste, A. D.; Koerner, H.; White, T. J. Synthesis of Elastomeric Liquid Crystalline Polymer Networks via Chain Transfer. *ACS Macro Lett.* **2017**, *6* (11), 1290−1295.
(25) Brannum, M. T.; Auguste, A. D.; Donovan, B. R.; Godman, N. P.; Matavulj, V. M.; Steele, A. M.; Korley, L. T. J.; Wnek, G. E.; White, T. J. Deformation and Elastic Recovery of Acrylate-Based Liquid Crystalline Elastomers. *Macromolecules* **2019**, *52*, 8248−8255.
(26) Hebner, T. S.; Fowler, H. E.; Herbert, K. M.; Skillin, N. P.; Bowman, C. N.; White, T. J. Polymer Network Structure, Properties, and Formation of Liquid Crystalline Elastomers Prepared via Thiol-Acrylate Chain Transfer Reactions. *Macromolecules* **2021**, *54* (23), 11074−11082.
(27) Hebner, T. S.; McCracken, J. M.; Bowman, C. N.; White, T. J. The Contribution of Oligomerization Reaction Chemistry to the Thermomechanical Properties of Surface-Aligned Liquid Crystalline Elastomers. *Macromolecules* **2023**, *56* (3), 974−979.
(28) Hebner, T. S.; Kirkpatrick, B. E.; Anseth, K. S.; Bowman, C. N.; White, T. J. Surface-Enforced Alignment of Reprogrammable Liquid Crystalline Elastomers. *Adv. Sci.* **2022**, *9*, No. 2204003.
(29) Javed, M.; Corazao, T.; Saed, M. O.; Ambulo, C. P.; Li, Y.; Kessler, M. R.; Ware, T. H. Programmable Shape Change in Semicrystalline Liquid Crystal Elastomers. *ACS Appl. Mater. Interfaces* **2022**, *14* (30), 35087−35096.
(30) Odian, G.*Step Polymerization*; Wiley, 2004; p 39.
(31) Hoyle, C. E.; Bowman, C. N. Thiol-Ene Click Chemistry. *Angew. Chem., Int. Ed.* **2010**, *49* (9), 1540−1573.
(32) Hoyle, C. E.; Lee, T. Y.; Roper, T. Thiol-Enes: Chemistry of the Past with Promise for the Future. *J. Polym. Sci., Part A: Polym. Chem.* **2004**, *42* (21), 5301−5338.
(33) Shaha, R. K.; Torbati, A. H.; Frick, C. P. Body-Temperature Shape-Shifting Liquid Crystal Elastomers. *J. Appl. Polym. Sci.* **2021**, *138* (14), No. 50136.
(34) Barnes, M.; Cetinkaya, S.; Ajnsztajn, A.; Verduzco, R. Understanding the Effect of Liquid Crystal Content on the Phase Behavior and Mechanical Properties of Liquid Crystal Elastomers. *Soft Matter* **2022**, *18* (27), 5074−5081.
(35) Bauman, G. E.; Hoang, J. D.; Toney, M. F.; White, T. J. Degree of Orientation in Liquid Crystalline Elastomers Defines the Magnitude and Rate of Actuation. *ACS Macro Lett.* **2023**, *12* (2), 248−254.
(36) Seddon, J. M. Structural Studies of Liquid Crystals by X-Ray Diffraction. In *Handbook of Liquid Crystals Set*; Wiley-VCH Verlag GmbH, 2008; pp 635−679.

https://doi.org/10.1021/acs.macromol.3c02291
Macromolecules 2024, 57, 2619−2627

(37) de Vries, A. X-ray Diffraction Studies of the Structure of the Skeweu Cybotactic Nematic Phase: A Review of the Literature. *J. Mol. Liq.* **1986**, *31* (4), 193−202.
(38) Francescangeli, O.; Laus, M.; Galli, G. Structure of the nematic mesophase with cybotactic groups in liquid-crystalline poly(urethane-ester)s. *Phys. Rev. E* **1997**, *55* (1), No. 481.
(39) Ware, T. H.; White, T. J. Programmed Liquid Crystal Elastomers with Tunable Actuation Strain. *Polym. Chem.* **2015**, *6* (26), 4835−4844.
(40) Saed, M. O.; Volpe, R. H.; Traugutt, N. A.; Visvanathan, R.; Clark, N. A.; Yakacki, C. M. High Strain Actuation Liquid Crystal Elastomers via Modulation of Mesophase Structure. *Soft Matter* **2017**, *13* (41), 7537−7547.
(41) Davidson, E. C.; Kotikian, A.; Li, S.; Aizenberg, J.; Lewis, J. A. 3D Printable and Reconfigurable Liquid Crystal Elastomers with Light-Induced Shape Memory via Dynamic Bond Exchange. *Adv. Mater.* **2020**, *32* (1), No. 1905682.
(42) Bispo, M.; Guillon, D.; Donnio, B.; Finkelmann, H. Main-Chain Liquid Crystalline Elastomers: Monomer and Cross-Linker Molecular Control of the Thermotropic and Elastic Properties. *Macromolecules* **2008**, *41* (9), 3098−3108.
(43) Kundler, I.; Finkelmann, H. Director Reorientation via Stripe-Domains in Nematic Elastomers: Influence of Cross-Link Density, Anisotropy of the Network and Smectic Clusters. *Macromol. Chem. Phys.* **1998**, *199* (4), 677−686.
(44) Choi, S.; Kim, B.; Park, S.; Seo, J. H.; Ahn, S. K. Slidable Cross-Linking Effect on Liquid Crystal Elastomers: Enhancement of Toughness, Shape-Memory, and Self-Healing Properties. *ACS Appl. Mater. Interfaces* **2022**, *14* (28), 32486−32496.
(45) Vernerey, F. J. Mechanics of Transient Semi-Flexible Networks: Soft-Elasticity, Stress Relaxation and Remodeling. *J. Mech. Phys. Solids* **2022**, *160*, No. 104776.
(46) Modes, C. D.; Bhattacharya, K.; Warner, M. Gaussian Curvature from Flat Elastica Sheets. *Proc. R. Soc. A* **2011**, *467* (2128), 1121−1140.

https://doi.org/10.1021/acs.macromol.3c02291
Macromolecules 2024, 57, 2619−2627